AIP | The Journal of Chemical Physics

Temperature and pressure dependence of ozone formation rates in the range 1–1000 bar and 90–370 K

H. Hippler, R. Rahn, and J. Troe

Citation: J. Chem. Phys. **93**, 6560 (1990); doi: 10.1063/1.458972
View online: http://dx.doi.org/10.1063/1.458972
View Table of Contents: http://jcp.aip.org/resource/1/JCPSA6/v93/i9
Published by the American Institute of Physics.

Temperature and pressure dependence of ozone formation rates in the range 1–1000 bar and 90–370 K

H. Hippler, R. Rahn, and J. Troe
Institut für Physikalische Chemie der Universität Göttingen, Tammannstrasse 6, D-3400 Göttingen, Germany

(Received 4 May 1990; accepted 21 June 1990)

The recombination $O + O_2 + M \rightarrow O_3 + M$ in the bath gases M = He, Ar, and N_2 was studied over the temperature range 90–370 K and the pressure range 1–1000 bar. The temperature and pressure dependences of the reaction rates show an anomalous behavior which is attributed to superpositions of mechanisms involving energy transfer, complex formation and participation of weakly bound electronically excited O_3 states. The results also show an analogy to oxygen isotope enhancements observed in ozone recombination and dissociation. Experiments in compressed liquid N_2 were also made showing a transition to diffusion control.

I. INTRODUCTION

Experimental studies of atom and radical recombination reactions at gas temperatures of the order of 100 K have rarely been performed.[1] Studies of hydrogen atom recombination by Walkauskas and Kaufman[2] at temperatures down to 77 K, and of ozone recombination

$$O + O_2 + M \rightarrow O_3 + M \tag{1}$$

by Rawlins, Caledonia, and Armstrong[3] at temperatures down to 80 K, are among the few exceptions. More radical recombination studies have been performed at temperatures down to 220 K, i.e., under stratospheric conditions (see evaluations in Ref. 4).

All of the existing low temperature studies were limited to pressures below 1 bar. In order to obtain conclusive information on the high pressure limit of the studied radical recombination reactions, experiments at low temperatures and higher pressures appear desirable. We demonstrate in the present work the feasibility of such experiments by studying a radical recombination reaction over the temperature range 90–370 K at pressures up to 1000 bar. The technology of such experiments is relatively simple and many more studies of this type should be performed.

At very low temperatures a number of interesting phenomena become apparent which are of smaller importance at higher temperatures: quantum effects become visible.[2,5] The radical-complex mechanism of atom recombination often dominates over the energy-transfer mechanism.[1] This mechanism may become observable also for radical recombination if the energy-transfer mechanism is sufficiently slow.[6] There may be other effects which have not yet been investigated in this context: Open-shell atoms and radicals often combine forming a large number of different electronic states. Generally only the few strongly bonding out of these electronic states provide a major contribution to the recombination rate.[7–9] At low temperatures, however, the weakly bonding states may also participate in the reaction. Increasing pressure may enhance this effect. At high pressures and low temperatures, the transition from normal gas phase recombination to a diffusion-controlled reaction is also of considerable interest.[10] The study of simple reaction systems of this kind appears particularly desirable for a comparison with theories (see the halogen atom recombinations which were studied in Refs. 11 and 12 at pressures up to 7 kbar). Continuing the room temperature studies of ozone recombination (1) from Ref. 6, which were limited to pressures below 200 bar, the present work aimed for the transition to diffusion control in a simple radical recombination system.

Low temperature and high pressure studies of ozone recombination (1) provide a number of additional attractions. The importance of this reaction in the atmosphere is well known (see the review of spectroscopic and kinetic data of the ozone system in Ref. 13). Studying temperature and pressure dependence over wide ranges might help to understand the anomalous rate constants of this reaction. Collisional energy transfer of vibrationally excited ozone was suggested to be very slow.[14] The contribution of metastable excited electronic states of this molecule has caused some controversy:[3,13,15] transient spectra, which were recorded during the early stages of the recombination, have been attributed either to metastable electronic states or to vibrationally highly excited ground state molecules. Quantum-chemical calculations (see, e.g., Refs. 16–21) have essentially been limited to equilibrium configurations, leaving uncertain the long-range parts of the potential energy surfaces.

High pressure recombination processes are in close relation to isotope exchange processes. This applies also to ozone recombination in relation to oxygen isotope exchange via $O + O_2 \rightarrow O_2 + O$. There are other interesting isotope effects in ozone recombination and thermal decomposition (see, e.g., Refs. 22–25). A recent study of the pressure dependence of heavy isotope enrichment in ozone recombination showed that the enrichment disappears at pressures of the order of 10 bar.[24] Likewise, the enrichment in ozone recombination shows an interesting temperature dependence.[25] If symmetry effects of various electronic states are the source for such isotope effects, then collisional coupling between the states may destroy isotope enrichments. On the other hand, collisional couplings be-

0021-9606/90/216560-10$03.00

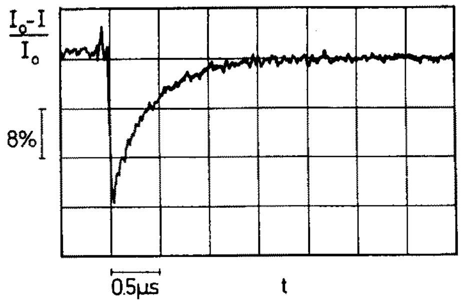

FIG. 1. Absorption-time profile of ozone recombination after O_3 photolysis (reaction mixture: 0.5 Torr O_3, 4.7 Torr O_2, 500 bar N_2; $T = 213$ K; photolysis wavelength 248 nm, analysis wavelength 265 nm; I = transmitted light intensity, I_o = incident light intensity).

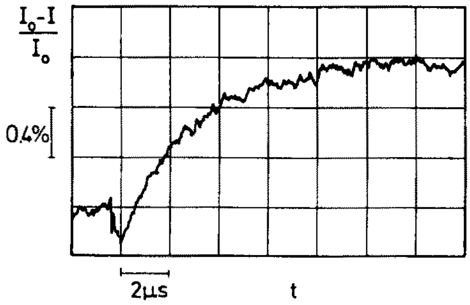

FIG. 3. Absorption-time profile of ozone formation after O_2 photolysis (reaction mixture: 100 Torr O_2, 10 bar N_2; $T = 300$ K; photolysis wavelength 193 nm, analysis wavelength 265 nm; I = transmitted light intensity, I_o = incident light intensity).

tween various electronic states will enhance high pressure recombination rates. Our present low temperature–high pressure recombination studies of reaction (1), therefore, may be directly related to the isotope enhancement measurements.

II. EXPERIMENTAL TECHNIQUE

Ozone recombination (1) in our work was investigated by laser flash photolysis. Oxygen atoms were generated by photolyzing O_2, N_2O, or O_3. The progress of the recombination was monitored via measurements of O_3 absorption signals. The experiments were carried out in a high pressure cell which could be cooled or heated over a wide temperature range. The components of our experimental setup will be described in more detail in the following.The high pressure cell was made from a stainless-steel rod of 12 cm length and 4 cm diam. A cylindrical reaction volume of 6 mm diam and 8 cm length was machined into this steel rod. It was closed at both ends by window disks of 14 mm diam and 5 mm thickness which were made either of quartz (for measurements down to 193 nm) or of sapphire (for measurements at 248 nm). The O rings for the windows were made of indium in order to keep elasticity at low temperatures. The reaction cell was designed for pressures up to 1.3 kbar. In order to prevent contact of O_3 with the wall, in experiments using O_3 as the oxygen source a thin teflon tube was laid into the stainless-steel reaction cell.

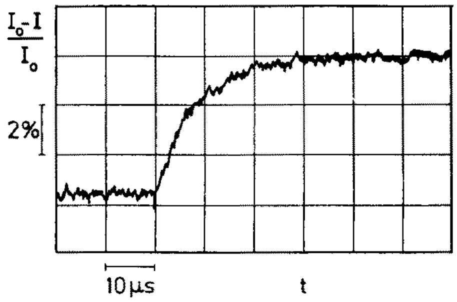

FIG. 2. Absorption-time profile of ozone formation after N_2O photolysis (reaction mixture: 81 Torr N_2O, 9.2 Torr O_2, 3.8 bar N_2, 178 bar Ar; $T = 373$ K; photolysis wavelength 193 nm, analysis wavelength 265 nm; I = transmitted light intensity, I_o = incident light intensity).

The reaction cell was surrounded by cooling-heating jacket made of a copper tube into which a heating wire was placed. A steady flow of liquid nitrogen was pressed through the copper tube. The minimum temperature achieved by this technique was 85 K, i.e., 8 K above the temperature of liquid nitrogen. Higher temperatures were reached by counter heating the wire in the tube. The accessible temperature range was 85–373 K. Temperatures in the cell were measured by a Pt-resistance thermometer. Nitrogen flow and heating current were automatically adapted to the desired experimental temperature. In order

TABLE I. Second-order recombination rate constants of ozone recombination (1) at different temperatures T and bath gas concentrations [M]; bath gas = He (D = self-diffusion coefficient of the bath gas, see Refs. 11 and 12).

T/K	p/bar	[He]/cm^{-3}	D^{-1}/s cm^{-2}	k/cm^3 s^{-1}
100	2	1.5×10^{20}	1.9×10^{1}	1.0×10^{-12}
	5	3.6×10^{20}	4.6×10^{1}	2.5×10^{-12}
	10	7.5×10^{20}	9.6×10^{1}	4.1×10^{-12}
	20	1.4×10^{21}	1.7×10^{2}	5.4×10^{-12}
	50	3.3×10^{21}	3.8×10^{2}	7.6×10^{-12}
	100	6.1×10^{21}	6.5×10^{2}	1.2×10^{-11}
	200	1.2×10^{22}	1.1×10^{3}	1.8×10^{-11}
	350	1.7×10^{22}	1.4×10^{3}	2.2×10^{-11}
	500	2.1×10^{22}	1.7×10^{3}	2.1×10^{-11}
	900	2.6×10^{22}	2.1×10^{3}	2.3×10^{-11}
140	5	2.6×10^{20}	3.1×10^{1}	4.3×10^{-13}
	10	5.2×10^{20}	6.0×10^{1}	7.7×10^{-13}
	20	1.1×10^{21}	1.2×10^{2}	1.3×10^{-12}
	50	2.6×10^{21}	2.8×10^{2}	2.6×10^{-12}
	100	5.0×10^{21}	4.9×10^{2}	4.5×10^{-12}
	200	8.8×10^{21}	8.0×10^{2}	6.6×10^{-12}
	500	1.8×10^{22}	1.3×10^{3}	1.1×10^{-11}
	900	2.4×10^{22}	1.9×10^{3}	1.5×10^{-11}
200	5	1.7×10^{20}	1.8×10^{1}	8.2×10^{-14}
	10	3.3×10^{20}	3.4×10^{1}	1.7×10^{-13}
	22	8.0×10^{20}	8.1×10^{1}	3.5×10^{-13}
	50	1.9×10^{21}	1.9×10^{2}	6.8×10^{-13}
	100	3.3×10^{21}	3.0×10^{2}	1.2×10^{-12}
	180	5.3×10^{21}	4.5×10^{2}	2.1×10^{-12}

to prevent condensation of moisture on the windows, the reaction cell with its cooling jacket was suspended in a vacuum vessel allowing the photolysis and analysis light to pass through external quartz windows. A number of additional precautions, which are not described here, had to be taken to minimize heat transfer.[26]

The bath gases M for reaction (1) were He, Ar, and N_2. These gases were of a purity better than 99.998%. Oxygen and other impurities were removed by a gas cleaning adsorber (Oxisorb, Messer-Griesheim). The bath gases were passed through a 3 μ-steel dust filter into an oil-free diaphragm compressor (MK 3000, Nova Swiss) and compressed up to 1 kbar. Ozone was prepared in an ozonizer and stored in a silica gel cooling trap. O_2 and N_2O were of purities better than 99.995% and 99%, respectively. (Obviously the purity problem requires particular attention in high pressure kinetics studies.)

Oxygen atoms were produced by photolyzing O_3 at 248 nm with a KrF excimer laser (Lambda Physik EMG 102, pulse energy 170 mJ, pulse width 16 ns) or by photolyzing O_2 at 193 nm with an ArF excimer laser (80 mJ, 11 ns). Alternatively, N_2O was photolyzed at 193 nm. Rapid electronic deactivaton of the nascent $O(^1D)$ was achieved by collisions with the bath gas N_2. The photolysis light was combined with the analysis light of dielectric mirrors and passed colinearly through the cylindrical reaction cell. The light source for absorption measurements was a Hg–Xe high pressure arc lamp (200 W Ushio UXM-200 H) which was pulsed for 80 μs during the photolysis experiment (intensity gain of a factor of 100). An electromagnetic shutter opened allowing access of the analysis light to the cell shortly before the laser flash. Absorption-time signals were recorded using a standard monochromator (Zeiss MM3), photomultiplier (RCA 1P28A) and digital storage oscilloscope (LeCroy 9400, band width 125 MHz). Five to twenty shots were averaged; blank and baseline signals were subtracted.

The concentration of the ozone formed by reaction (1) was measured at 265 nm. This wavelength has several advantages: the absorption coefficient ($\sigma = 9 \times 10^{-18}$ cm^2) is large, the Hg–Xe lamp has a high intensity, and the O_3 absorption spectrum here is nearly excitation independent[27] so that relaxation processes do not interfere.

The oxygen atom sources O_3, N_2O, and O_2 had different ranges of applicability. Because of the small absorption coefficient of O_2 at 193 nm, experiments with O_2/bath gas mixtures required extensive averaging (more than 200 shots). This in turn led to accumulation of O_3 which also is photolyzed at 193 nm; hence, the range of accessible concentration conditions was limited. N_2O photolysis at 193 nm avoids this problem and provides a clean $O(^3P)$ source under the condition that a sufficient amount of N_2 is added for the electronic quenching of $O(^1D)$. Since the vapor pressure of N_2O gets too small at temperatures below 150 K, gas phase experiments here became difficult. However, N_2O dissolves well in liquid N_2 such that experiments with this oxygen source could well be conducted in compressed liquid N_2 up to 1 kbar at 90 K. O_3 photolysis at 248 nm permitted gas phase experiments down to 90 K without problems. Some N_2 was always added for the electronic quenching of $O(^1D)$. Typical reaction mixtures then contained 0.5 Torr O_3, 2–15 Torr O_2, 1–3 bar N_2, and the bath gas M at pressures up to 1 kbar.

III. EXPERIMENTAL RESULTS

The recorded absorption-time profiles all corresponded to a clean reaction behavior which could be exclusively attributed to reaction (1). The reaction always was observed under pseudo-first-order conditions such that the second-order rate coefficient k could easily be derived. Figure 1 shows the example of an absorption-time profile for ozone recombination after photolysis of an $O_3/O_2/N_2$ mixture. Figure 2 shows ozone formation after photolysis of an $N_2O/O_2/N_2/Ar$ mixture. Figure 3 shows the corresponding signal for an O_2/N_2 mixture.

The derived rate constants k are summarized in Tables I–III. k values are given for selected values of [M]. Since high values of [M] were studied, we also indicate the corresponding values of the inverse of the self-diffusion coefficients D of the bath gas [M]. Our earlier high pressure experiments suggested[10–12] that a D^{-1} scale conveniently describes the transition from gas to liquid phase, in particular if the transition to a diffusion controlled reaction is considered.

Figures 4–6 illustrate the results from Tables I–III by a double-logarithmic falloff representation. The three bath gases He, Ar, and N_2 show notable differences and "anomalous falloff behavior." At low pressures the curves seem to lead from the low pressure third-order to a high pressure second-order range in the normal way. A conventional falloff extrapolation, therefore, was made in Ref. 6 on the basis of room temperature experiments at pressures up to 200 bar. However, at pressures above this range a dramatic turn-up of the rate constants sets in which leads to high pressure rate constants more than an order of magnitude higher than extrapolated from lower pressures. At the highest densities achieved, the rate constants decrease again indicating the transition to diffusion control. The representation of k as a function of D^{-1} better illustrates this transition (see Fig. 7 for $M = N_2$). Compared to the corresponding transition in halogen atom recombination,[11,12] a less abrupt transition with a broad intermediate plateau in the $k - D^{-1}$ representation is observed. The 130 K curve in Fig. 7 combines gas phase results at 130 K with liquid phase results at 90–120 K which appears tolerable in the diffusion controlled range, see below.

The separate representation of the temperature dependence of the low pressure third-order rate constants is also illustrative. Figures 8–10 combine the present results with low pressure results from other laboratories, and with high temperature dissociation results which have been converted to recombination results by means of the equilibrium constant. Large temperature ranges have been covered, e.g., the range 80–3000 K for $M = Ar$ (corresponding to $4 \leqslant E_O/RT \leqslant 150$ were E_O = dissociation energy of O_3). There is excellent agreement between the

TABLE II. As Table I; bath gas = Ar.

T/K	p/bar	[Ar]/cm^{-3}	D^{-1}/s cm^{-2}	k/cm^3 s^{-1}
100	200	1.55×10^{22}	1.5×10^{4}	2.1×10^{-11}
	500	1.60×10^{22}	1.6×10^{4}	2.0×10^{-11}
163	7	3.4×10^{20}	8.6×10^{1}	6.5×10^{-13}
	20	1.0×10^{21}	2.6×10^{2}	2.0×10^{-12}
	50	3.7×10^{21}	1.0×10^{3}	7.8×10^{-12}
	350	1.7×10^{22}	1.2×10^{4}	2.1×10^{-11}
	800	2.0×10^{22}	2.0×10^{4}	2.0×10^{-11}
213	10	3.5×10^{20}	8.6×10^{1}	3.0×10^{-13}
	21	7.4×10^{20}	1.8×10^{2}	6.0×10^{-13}
	50	2.0×10^{21}	5.0×10^{2}	1.3×10^{-12}
	100	4.6×10^{21}	1.2×10^{3}	2.1×10^{-12}
	180	8.3×10^{21}	2.5×10^{3}	3.5×10^{-12}
	500	1.5×10^{22}	6.6×10^{3}	7.5×10^{-12}
	1000	1.8×10^{22}	1.1×10^{4}	1.1×10^{-11}
253	9	2.5×10^{20}	6.0×10^{1}	1.4×10^{-13}
	19	5.6×10^{20}	1.3×10^{2}	2.5×10^{-13}
	31	9.0×10^{20}	2.1×10^{2}	4.0×10^{-13}
	50	1.5×10^{21}	3.5×10^{2}	5.3×10^{-13}
	100	3.2×10^{21}	7.6×10^{2}	9.4×10^{-13}
	180	5.8×10^{21}	1.5×10^{3}	1.6×10^{-12}
	350	1.0×10^{22}	3.0×10^{3}	3.5×10^{-12}
	500	1.3×10^{22}	4.3×10^{3}	5.0×10^{-12}
	1000	1.6×10^{22}	7.2×10^{3}	7.8×10^{-12}
300	9	2.2×10^{20}	5.0×10^{1}	8.6×10^{-14}
	21	5.1×10^{20}	1.2×10^{2}	1.7×10^{-13}
	30	7.2×10^{20}	1.6×10^{2}	2.2×10^{-13}
	50	1.2×10^{21}	2.7×10^{2}	3.0×10^{-13}
	70	1.7×10^{21}	3.8×10^{2}	3.9×10^{-13}
	100	2.2×10^{21}	4.9×10^{2}	5.5×10^{-13}
	170	4.1×10^{21}	9.3×10^{2}	7.4×10^{-13}
	350	8.0×10^{21}	2.0×10^{3}	1.4×10^{-12}
	500	1.0×10^{22}	2.7×10^{3}	2.5×10^{-12}
	1000	1.5×10^{22}	5.1×10^{3}	4.6×10^{-12}
373	10	1.95×10^{20}	4.2×10^{1}	5.6×10^{-14}
	20	3.9×10^{20}	8.4×10^{1}	9.0×10^{-14}
	50	9.7×10^{20}	2.1×10^{2}	2.0×10^{-13}
	100	2.0×10^{21}	4.2×10^{2}	3.6×10^{-13}
	180	3.4×10^{21}	7.0×10^{2}	4.6×10^{-13}

TABLE III. As Table I; bath gas = N_2.

T/K	p/bar	[N_2]/cm^{-3}	D^{-1}/s cm^{-2}	k/cm^3 s^{-1}
90	80	1.73×10^{22}	2.8×10^{4}	1.9×10^{-11}
	180	1.78×10^{22}	3.1×10^{4}	1.9×10^{-11}
	1000	2.0×10^{22}	4.8×10^{4}	1.5×10^{-11}
100	1	7.0×10^{19}	2.3×10^{1}	6.7×10^{-13}
	70	1.55×10^{22}	1.7×10^{4}	2.0×10^{-11}
	190	1.68×10^{22}	2.3×10^{4}	2.0×10^{-11}
110	70	1.45×10^{22}	1.3×10^{4}	2.1×10^{-11}
	180	1.55×10^{22}	1.6×10^{4}	2.1×10^{-11}
120	70	1.30×10^{22}	8.6×10^{3}	1.9×10^{-11}
	180	1.46×10^{22}	1.2×10^{4}	1.9×10^{-11}
130	3	1.7×10^{20}	5.2×10^{1}	7.3×10^{-13}
	6	3.5×10^{20}	1.1×10^{2}	1.5×10^{-12}
	13	8.3×10^{20}	2.5×10^{2}	3.8×10^{-12}
	22	1.6×10^{21}	4.6×10^{2}	6.3×10^{-12}
	30	3.2×10^{21}	9.2×10^{2}	1.0×10^{-11}
	50	1.0×10^{22}	4.3×10^{3}	1.8×10^{-11}
	100	1.3×10^{22}	7.4×10^{3}	1.9×10^{-11}
	180	1.4×10^{22}	1.0×10^{4}	1.8×10^{-11}
173	2	9.6×10^{19}	2.8×10^{1}	2.0×10^{-13}
	6	2.7×10^{20}	7.5×10^{1}	4.9×10^{-13}
	10	4.4×10^{20}	1.2×10^{2}	7.0×10^{-13}
	20	9.7×10^{20}	2.7×10^{2}	1.3×10^{-12}
	50	2.7×10^{21}	7.1×10^{2}	3.2×10^{-12}
	100	5.6×10^{21}	1.5×10^{3}	6.2×10^{-12}
	190	1.0×10^{22}	3.6×10^{3}	1.1×10^{-11}
	350	1.2×10^{22}	5.6×10^{3}	1.5×10^{-11}
	500	1.4×10^{22}	7.8×10^{3}	1.7×10^{-11}
	1000	1.6×10^{22}	1.2×10^{4}	2.1×10^{-11}
213	3	8.6×10^{19}	2.3×10^{1}	1.1×10^{-13}
	5	1.8×10^{20}	4.9×10^{1}	2.1×10^{-13}
	10	3.5×10^{20}	9.4×10^{1}	3.7×10^{-13}
	15	4.9×10^{20}	1.3×10^{2}	5.6×10^{-13}
	20	7.2×10^{20}	1.9×10^{2}	6.8×10^{-13}
	30	1.1×10^{21}	2.9×10^{2}	9.5×10^{-13}
	60	2.1×10^{21}	5.1×10^{2}	1.8×10^{-12}
	100	3.9×10^{21}	9.4×10^{2}	2.8×10^{-12}
	180	6.8×10^{21}	1.7×10^{3}	5.1×10^{-12}
	350	1.0×10^{22}	3.1×10^{3}	8.5×10^{-12}
	500	1.2×10^{22}	4.5×10^{3}	1.1×10^{-11}
	1000	1.5×10^{22}	8.0×10^{3}	1.6×10^{-11}
253	3	7.3×10^{19}	1.9×10^{1}	6.2×10^{-14}
	6	1.7×10^{20}	4.4×10^{1}	1.4×10^{-13}
	10	2.9×10^{20}	7.4×10^{1}	2.2×10^{-13}
	20	5.8×10^{20}	1.5×10^{2}	4.0×10^{-13}
	50	1.5×10^{21}	3.5×10^{2}	7.8×10^{-13}
	90	2.9×10^{21}	6.7×10^{2}	1.2×10^{-12}
	140	4.0×10^{21}	9.0×10^{2}	1.8×10^{-12}
	200	5.5×10^{21}	1.2×10^{3}	2.4×10^{-12}
	350	8.2×10^{21}	2.0×10^{3}	4.0×10^{-12}
	500	1.0×10^{22}	2.8×10^{3}	5.7×10^{-12}
	1000	1.3×10^{22}	4.7×10^{3}	9.3×10^{-12}
300	5	1.2×10^{20}	2.9×10^{1}	5.9×10^{-14}
	10	2.4×10^{20}	5.8×10^{1}	1.2×10^{-13}
	20	4.8×10^{20}	1.1×10^{2}	2.4×10^{-13}
	50	1.2×10^{21}	2.8×10^{2}	5.4×10^{-13}
	65	1.5×10^{21}	3.4×10^{2}	6.0×10^{-13}
	100	2.4×10^{21}	5.3×10^{2}	7.6×10^{-13}
	170	3.5×10^{21}	7.5×10^{2}	9.0×10^{-13}
	200	4.2×10^{21}	8.8×10^{2}	1.0×10^{-12}
	350	6.8×10^{21}	1.4×10^{3}	1.5×10^{-12}
	500	9.3×10^{21}	2.2×10^{3}	2.0×10^{-12}
	1000	1.2×10^{22}	3.5×10^{3}	3.9×10^{-12}
373	10	1.95×10^{20}	4.4×10^{1}	6.6×10^{-14}
	20	3.9×10^{20}	8.7×10^{1}	1.2×10^{-13}
	50	1.05×10^{21}	2.3×10^{2}	2.9×10^{-13}
	100	1.9×10^{21}	3.9×10^{2}	4.0×10^{-13}
	180	3.4×10^{21}	6.7×10^{2}	6.1×10^{-13}

different laboratories. The agreement between the low temperature data from Ref. 3 and our work for M = Ar should be mentioned in particular. There is a pronounced increase of the negative temperature coefficients, n, with decreasing temperatures (n being defined by $k \propto T^{-n}$). However, the three bath gases differ in this regard: Whereas the change in n occurs near 500 K for M = Ar and N_2, it occurs near 200 K for M = He. The following representations of k have been derived from the results shown in Figs. 8–10:

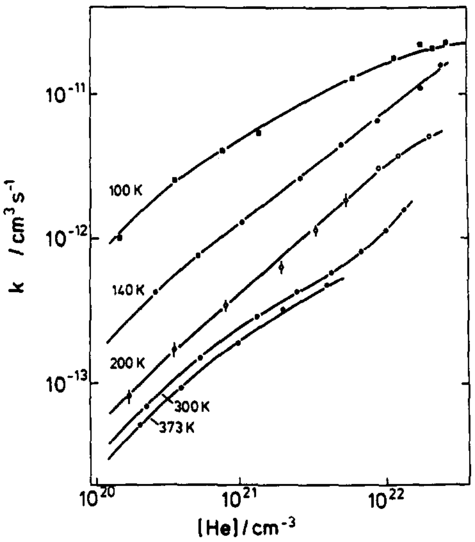

FIG. 4. Dependence of the second-order rate coefficients k for ozone recombination (1) on temperature and bath gas concentration in the bath gas He.

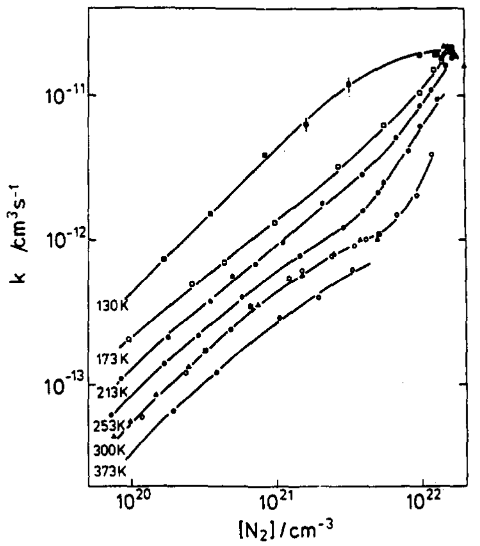

FIG. 6. As Fig. 5, in the bath gas N_2.

M = He: $k = [\mathrm{He}]\ 7.2\times10^{-33}\ (T/100\ \mathrm{K})^{-3.7}\ \mathrm{cm^6\,s^{-1}}$ at 100–200 K,

$k = [\mathrm{He}]\ 3.4\times10^{-34}\ (T/300\ \mathrm{K})^{-1.2}\ \mathrm{cm^6\,s^{-1}}$ at 200–1000 K;

M = Ar: $k = [\mathrm{Ar}]\ 8.0\times10^{-33}\ (T/100\ \mathrm{K})^{-3.2}\ \mathrm{cm^6\,s^{-1}}$ at 80–150 K,

$k = [\mathrm{Ar}]\ 4.5\times10^{-34}\ (T/300\ \mathrm{K})^{-2.7}\ \mathrm{cm^6\,s^{-1}}$ at 150–400 K,

$k = [\mathrm{Ar}]\ 4.0\times10^{-35}\ (T/1000\ \mathrm{K})^{-1.0}\ \mathrm{cm^6\,s^{-1}}$ at 700–3000 K;

M = N_2: $k = [\mathrm{N_2}]\ 5.5\times10^{-34}\ (T/300\ \mathrm{K})^{-2.6}\ \mathrm{cm^6\,s^{-1}}$ at 100–400 K,

$k = [\mathrm{N_2}]\ 5.2\times10^{-35}\ (T/1000\ \mathrm{K})^{-1.3}\ \mathrm{cm^6\,s^{-1}}$ at 700–900 K.

IV. DISCUSSION

The observed temperature and pressure dependences of ozone recombination look unusual. The following features appear most noticeable:

(i) The low pressure rate constants k_0 have pronounced negative temperature coefficients ($k_0/[\mathrm{M}] \propto T^{-n}$), with n being much larger at low than at high temperatures.

(ii) The ordering of the low pressure rate constants for different bath gases changes with temperature. The

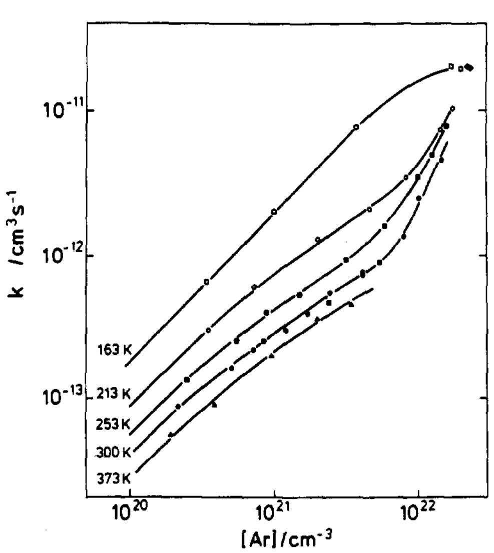

FIG. 5. As Fig. 5, in the bath gas Ar.

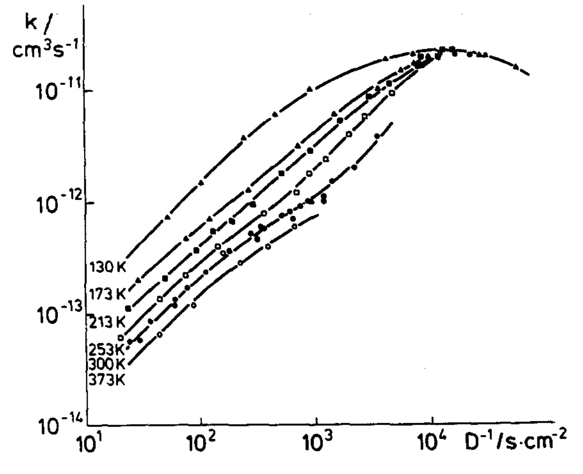

FIG. 7. As Fig. 6, but representation as a function of the inverse self-diffusion coefficient D of N_2 (experiments from this work, in addition results from Ref. 6: ⊙ and Ref. 28: ⊗ at 300 K; experiments in compressed liquid N_2: ⊠: 120 K, ◪: 110 K, ⊕: 100 K and ▲: 90 K).

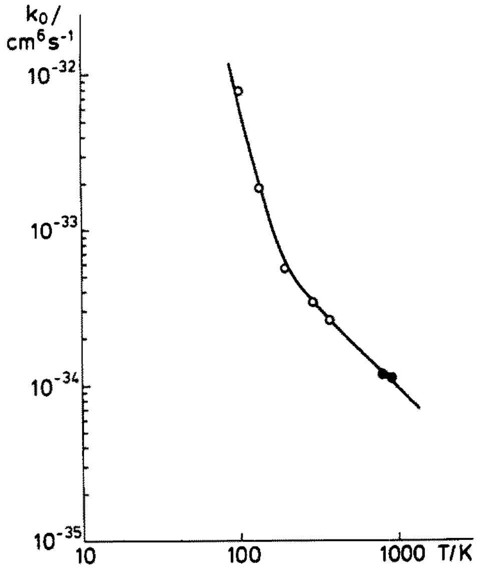

FIG. 8. Temperature dependence of the third-order rate coefficients k/[M] for ozone recombination (1) in M = He (○: this work, ●: Ref. 30).

k_0/[M] values are nearly equal at 100 K, being 7.0×10^{-33}, 8.0×10^{-33}, and 8.7×10^{-33} $cm^6 s^{-1}$ for M = He, Ar, and N_2, respectively; at 300 K they are 3.4×10^{-34}, 4.0×10^{-34}, and 5.6×10^{-34} $cm^6 s^{-1}$, whereas at 1000 K they change into 10.0×10^{-35}, 4.0×10^{-35}, and 5.2×10^{-35} $cm^6 s^{-1}$ for M = He, Ar, and N_2, respectively.

(iii) The falloff curves show an S-shaped form. The S structure is most pronounced near 300 K and nearly absent near 100 K.

(iv) At temperatures close to 100 K the second order rate constant k decreases at the highest densities, indicating a transition to diffusion control.[10–12] A broad intermediate plateau between the rise and the fall of the rate constant is observed, if a presentation of the second-order rate constant k as a function of the inverse self-diffusion coefficient of the solvent is chosen.

One may try to interpret the observed properties of the rate constants in several ways. We consider three mechanisms to explain the low and medium density results: First, we try to relate our observations with the falloff curves of the energy transfer mechanism of normal dissociation–recombination reactions. Second, we take into account contributions from the radical-complex mechanism of recombination processes, such as discussed for atom recombination reactions. Third, we investigate a recombination pathway involving excited electronic states of ozone. These three possibilities will be inspected in the following with respect to their temperature, pressure, and bath gas dependences.

Energy-transfer mechanism (ET): If ozone recombination in the temperature range 100–400 K would follow the normal energy-transfer mechanism (ET) of dissociation–recombination reactions, standard unimolecular rate theory should apply. Under the condition that a single electronic state, correlating O and O_2 with O_3 in the electronic ground states contributes to the reaction, the low pressure rate constant would be given by

$$k_0=[\mathrm{M}]\beta_c Z_{\mathrm{LJ}} \times\left(\frac{h^2}{2\pi\mu kT}\right)^{3/2}\frac{Q_{\mathrm{rot}}(\mathrm{O}_3)}{Q_{\mathrm{vib}}(\mathrm{O}_2)Q_{\mathrm{rot}}(\mathrm{O}_2)}\frac{Q_{\mathrm{el}}(\mathrm{O}_3)}{Q_{\mathrm{el}}(\mathrm{O}_2)Q_{\mathrm{el}}(\mathrm{O})} \times\rho_{\mathrm{vib},h}(E_0)kT\,F_E F_{\mathrm{anh}} F_{\mathrm{rot}} F_{E_Z},$$

with the symbols explained in Ref. 29. The evaluation of the various factors in this equation is straightforward and, for the O_3 system, has been done in Refs. 29–31. A comparison with the experimental dissociation results at $T \geqslant 800$ K leads to small collision efficiencies β_c which correspond[29] to energy transfer step sizes of the order of

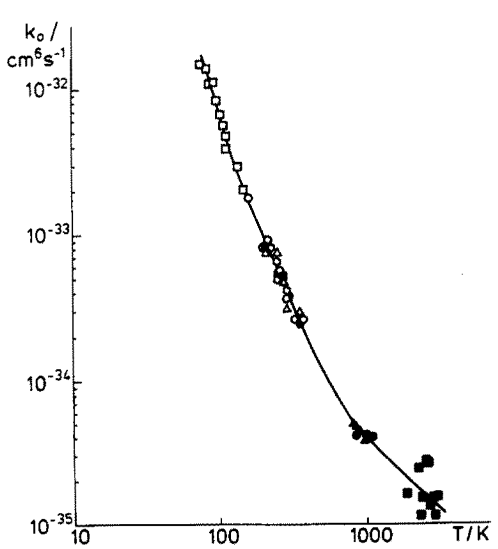

FIG. 9. As Fig. 8, but in M = Ar (○: this work, □: Ref. 3, ●: Ref. 30, △: Ref. 46, ⬡: Ref. 47, ⊠: Ref. 48, ⊗ Ref. 49, ▲: Ref. 50, ■: Ref. 51).

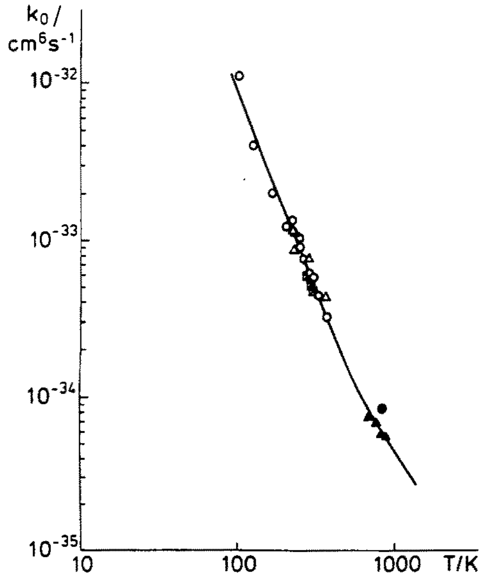

FIG. 10. As Fig. 8, but in M = N_2 (○: this work, ●: Ref. 30, △: Ref. 46, ⬡: Ref. 47, ⊠: Ref. 48, ▲: Ref. 50).

$\langle \Delta E \rangle = -(20 \pm 10)$ cm^{-1} for M = He, Ar, and N_2. These small values are consistent with the observation of inefficient collisional energy transfer made in the classical trajectory calculations of Ref. 14. One may attribute this behavior to the high vibrational frequencies of O_3 in comparison to the small dissociation energy E_0 and, hence, the small harmonic oscillator density of states $\rho_{\mathrm{vib},h}(E_0)$ at E_0. The temperature dependence of the strong collision limit of k_0 (i.e., $\beta_c = 1$) between 200 and 400 K would correspond to[29] $n \approx -0.5$ if $F_E = 1$ (or to $n \approx +0.7$ if adiabatic zero-point barriers are included, i.e., $F_E < 1$; the appearance of these barriers strongly depends on the potential; in the absence of further information we leave out this effect). The collision efficiency β_c will not have a strong temperature dependence either: if $\langle \Delta E \rangle \propto T$ such as observed for energy transfer in SO_2 and CS_2,[32] $\beta_c \approx -\langle \Delta E \rangle / F_E kT$ would be independent of temperature;[29] with constant $\langle \Delta\ E \rangle$, β_c would be proportional to T^{-1}. Replacing the Lennard-Jones collision frequency Z_{LJ} by an energy-transfer collision frequency Z_{ET}, such as suggested in Ref. 33, also does not change the temperature dependence of k_0 much. We, therefore, conclude that our present knowledge about the temperature dependence of the ET mechanism would lead to $k_0 \propto T^{-1(\pm 0.5)}$ which is in marked contrast to the observations of ozone recombination in Ar and N_2 at $T < 400$ K. Nevertheless, the ET mechanism apparently becomes dominant at $T > 500$ K for these bath gases, where the experimental values of k_0 approach a T^{-1} dependence in agreement with the corresponding theoretical predictions.[29] For the bath gas He, the ET mechanism apparently operates between 200 and 900 K where $k_0 \propto T^{-1}$ is observed.

Radical-complex mechanism (RC): Because of the unusually inefficient energy transfer in highly excited ozone, in Ref. 6 we suggested a contribution of the radical complex mechanism (RC) to ozone recombination. Choosing the simple formulation

$$O + M \rightleftarrows OM, \tag{2}$$

$$O_2 + M \rightleftarrows O_2M, \tag{3}$$

$$O_2 + OM \rightarrow O_3 + M, \tag{4}$$

$$O + O_2M \rightarrow O_3M, \tag{5}$$

$$O_2M + OM \rightarrow O_3 + 2M, \tag{6}$$

the second-order rate constant for ozone formation is given by

$$k = \frac{(K_2 k_4 + K_3 k_5)[\mathrm{M}] + K_2 K_3 k_6 [\mathrm{M}]^2}{1 + (K_2 + K_3)[\mathrm{M}] + K_2 K_3 [\mathrm{M}]^2}, \tag{7}$$

where K_2 and K_3 denote equilibrium constants. In the low pressure limit one would have

$$k_0 = (K_2 k_4 + K_3 k_5)[\mathrm{M}]. \tag{8}$$

The Lennard-Jones parameters for O–M and O_2–M complexes are known to be[34,35] ϵ/k = 24–29, 90–95, and 107 K for O–He, O–Ar, and O–N_2 and 29, 130, and 123–128 K for O_2–He, O_2–Ar, and O_2–N_2, respectively, whereas σ = 3.27–3.08, 3.6–3.48, and 3.41 Å for O_2–He, O_2–Ar, and O_2–N_2, and 3.44, 3.62, and 3.69–3.63 Å for O_2–He, O_2–Ar, and O_2–N_2, respectively. We estimate the equilibrium constants K_2 and K_3 on the basis of these parameters and the simple Bunker–Davidson expression[36,37]

$$K \approx \sqrt[3]{\pi} \left(\frac{\epsilon}{kT} \right)^{3/2} \left[\frac{8}{3} + \frac{32}{45} \frac{\epsilon}{kT} \right], \tag{9}$$

which approaches a $K \propto T^{-5/2}$ temperature dependence at $\epsilon > kT$ [deviations from Eq. (9) are expected for M = He]. At $T \approx 300$ K, Eq. (9) leads to $K_2 \approx K_3 \approx \sigma^3 \approx 4.3 \times 10^{-23}$ cm^3 for M = Ar and N_2 such that the comparison with the experimental k_0 values near 300 K would require $k_4 + k_5 \approx 1.2 \times 10^{-11}$ cm^3 s^{-1}. Although systematic studies of the rate constants for exchange processes with van der Waals complexes are not available, it appears not unreasonable to approximate k_4, k_5, and k_6 by the capture (or high pressure recombination) rate constants of O + O_2 in the electronic ground state. A value of 2.7×10^{-12} cm^3 s^{-1} (originally based[6] on a falloff extrapolation at 300 K from pressures below 200 bar) in Refs. 9 and 31 was well accounted for by SACM unimolecular rate theory (as long as adiabatic zero-point barriers are neglected). While the pressure dependence of the rate constants at 300 and 400 K and pressures below 200 bar can be represented in this way by the RC mechanism, neither the sharp turn up at higher pressures nor the S structures and the large values of the rate constants at lower temperatures can be explained. The underestimate of the temperature dependence of k_0 by K from Eq. (9) might be due to the oversimplified form of this equation (for a more detailed treatment of equilibrium constants of complexes see Ref. 38). However, the large high pressure values at low T clearly exceed O + O_2 capture rate constants which have probably only a mild temperature dependence.

The ozone recombination in the bath gas He shows a markedly different temperature dependence in the low pressure limit. The $k_0 \propto T^{-1}$ dependence between 200 and 900 K suggests that the ET mechanism here still dominates over the RC mechanism because the values of K_2 and K_3 are small. Estimating K_2 and K_3 by Eq. (9) (in spite of the limitations of this expression for M = He and H_2, see Ref. 36), confirms this interpretation, which is in complete analogy to the situation of the recombination of iodine atoms.[37] At temperatures below 200 K apparently the mechanism, which is responsible for the high presure turn-up, has shifted so much towards lower pressures that this mechanism governs the low pressure range as well, see below.

Mechanism involving excited electronic states (EE): The foregoing discussions have suggested that the energy transfer mechanism is only of minor importance at low temperatures. The radical complex mechanism, on the other hand, can only account for part of the observations. Looking for other mechanisms, in the following we consider a recombination pathway involving weakly bonding excited electronic states of ozone. The low-lying[16] $O_3(^3B_2)$ state may be a candidate for this mechanism (EE). At high temperatures, the excited electronic states redissociate rapidly such that the ET mechanism dominates unless very high pressures are applied. Discrepancies between O disappearance and O_3 vibrational ground state appearance in ozone recombination recently have also been attributed[15] to a pathway involving metastable electronically excited states of O_3. These observations have been made at various wavelengths in the Hartley band. Unfortunately, vibrational excitation strongly modifies the spectrum[27] such that slow vibrational deactivation also can cause delayed appearance of the "cold" spectrum. Likewise, the attribution of changes of the spectrum during recombination to metastable electronic states[39,40] appears ambiguous because of the strong influence of vibrational excitation on the UV absorption of O_3. Unless the metastable electronic state of O_3 has a considerably large bond energy, its rapid redissociation would reduce the stationary concentration and the trapping capacity of this state. It nevertheless may manifest its presence in the recombination rates such as discussed in the following.

Denoting weakly bonding electronically excited states by $O_3(A)$ and electronic ground state by $O_3(X)$, we consider a mechanism

$$O + O_2 \rightarrow O_3(A), \tag{10}$$

$$O_3(A) \rightarrow O + O_2, \tag{11}$$

$$O_3(A) + M \rightarrow O_3(X) + M, \tag{12}$$

which gives a rate constant

$$k = \frac{k_{10}k_{12}[M]}{k_{11} + k_{12}[M]}. \tag{13}$$

In the low pressure limit, the expression of $k_0 = k_{10}k_{12}[M]/k_{11}$ includes the equilibrium constant $K_{10} = k_{10}/k_{11}$ for the $O + O_2 \rightarrow O_3(A)$ equilibrium. In the absence of more detailed knowledge of the $O_3(A)$ potential, K_{10} is difficult to estimate. Lennard-Jones parameters for $O + O_2$ interaction of $\epsilon/k = 107$ K and $\sigma = 33.8$ Å were derived from scattering results,[35] probably representing an average over a manifold of interactions. The estimate of K_{10} via Eq. (9), therefore, will only provide a lower limit. Likewise, the calculation of the collision-induced electronic transition rate constant k_{12} via the formalism of Refs. 41 and 42 would require detailed knowledge about the $O_3(A)$ and $O_3(X)$ potentials which is not available. Neglecting a temperature dependence of k_{12}, Eq. (9) like in the RC mechanism would account for a temperature dependence of $k_0 \propto T^{-5/2}$. The high pressure limiting value k_{10} of Eq. (13) may well differ from the discussed values k_4, k_5, and k_6 of the RC mechanism. With a potential, which is much flatter in $O_3(A)$ than in $O_3(X)$, larger values of the centrifugal partition function Q^*_{cent} and of the rigidity factor $f_{\text{rec},\infty}$ in the high pressure recombination rate constant are expected.[9,31] Therefore, our k values larger than 2×10^{-11} cm^3 s^{-1} could be accounted for by the EE mechanism. Nevertheless, the simple falloff expression of Eq. (13) is also unable to explain the observed S-shaped structures of the pressure dependence of k. The leveling off of the rate constant near 100 K at $[M] \geqslant 10^{22}$ cm^{-3} could even completely be attributed to the transition to diffusion control if k_{10} would exceed 2×10^{-11} cm^3 s^{-1}, see below.

So far, neither the EE mechanism [Eq. (13)] nor the sum of the EE and the RC mechanism [Eqs. (13) and (7)] appear able to explain the observed S shape of the falloff curves. The measurements suggest an acceleration of the reaction which is more than proportional to the pressure and gains importance at lower temperatures. We propose that this is a mechanism involving collision-induced electronic transitions in van der Waals clusters (EE–RC). Clustering of O_3 may lead to different shifts of the potential curves of the $O_3(A)$ and $O_3(X)$ states such that transitions are facilitated. Collisions of $O_3M(A)$ with M then may lead to larger electronic transition rates than reaction (12). Therefore, to reactions (10)–(12) we add the steps

$$O_3(A) + M \rightarrow O_3M(A), \tag{14}$$

$$O_3M(A) \rightarrow O_3(A) + M, \tag{15}$$

$$O_3M(A) + M \rightarrow O_3(X) + 2M, \tag{16}$$

which leads to the rate constant

$$k = k_{10}\frac{k_{12}[M] + k_{14}k_{16}[M]^2/(k_{15} + k_{16}[M])}{k_{11} + k_{12}[M] + k_{14}k_{16}[M]^2/(k_{15} + k_{16}[M])}. \tag{17}$$

If k_{12} is neglected, $k_{16}[M] \ll k_{15}$, and $k_{14}[M] \ll k_{11}$, Eq. (17) leads to

$$k = \frac{k_{10}}{k_{11}}\frac{k_{14}}{k_{15}}k_{16}[M]^2. \tag{18}$$

Estimating k_{10}/k_{11} and k_{14}/k_{15} by Eq. (9) with Lennard-Jones parameters such as given above, leads to temperature dependences of k in Eq. (18) which are between T^{-3} and T^{-5} (in addition to the temperature dependence of k_{16}). The strong shift of the high pressure turnup of k towards lower pressures, if the temperature is decreased, would be consistent with this model. Tentatively we, therefore, assume that an EE–RC mechanism at low temperatures in addition to the RC mechanism contributes to the recombination rate. Evaluating the magnitude of the turnup at 300 K leads to values of the rate constant k_{16} of the order of 10^{-11} cm^3 s^{-1} if $(k_{10}/k_{11})(k_{14}/k_{15}) \approx 2\times 10^{-45}$ cm^{-6} is assumed.

At low temperatures the marked turnups of the rate constants disappear. Such effects are included in the rate constant expression of Eq. (17). They indicate that k_{15} falls below $k_{16}[M]$. For M = Ar and N_2 this apparently happens in the temperature range 130–170 K with $[M] \approx (10^{21}$–$10^{22})$ cm^{-3}. At the same time k_{11} may fall below $k_{14}[M]$. With similar bond energies of O_2–$O(A)$ and $O_3(A)$–M, the two effects become nonseparable, enhancing each other, such that a relatively abrupt change from normal falloff behavior into sharp turnups arises.

A model superposing the EE–RC and the RC mechanisms for M = Ar and N_2, or the EE–RC and the ET mechanisms for M = He, in spite of its oversimplification unfortunately contains too many adjustable parameters for a unique fit. Nevertheless, the proposed scheme is in qualitative agreement with the observations.

Transition to a diffusion controlled recombination: In previous experimental studies of atom recombination rates in the gas–liquid transition range,[10–12] the rate constant k could well be represented by

$$1/k \approx 1/k_{\text{gas}} + 1/k_{\text{diff}}, \tag{19}$$

where k_{gas} denotes the gas phase rate constant and k_{diff} is the rate constant of the diffusion-controlled process. At high densities k_{gas} is obtained from the conventional gas phase expression by modifying [M] in the following way: [M] is replaced by a "corrected" concentration $[\text{M}]_{\text{corr}}$ given by

$$[\text{M}]_{\text{corr}} = [\text{M}]_0[D^{-1}([\text{M}])/D^{-1}([\text{M}])_0]. \tag{20}$$

$[\text{M}]_0$ denotes a sufficiently low bath gas concentration in the range where the inverse self-diffusion coefficient D^{-1} is proportional to the concentration.[10–12] In the previous sections we have discussed models for k_{gas}. We now combine these expressions with models for the diffusion-controlled reaction. We approximate k_{diff} by[10–12]

$$k_{\text{diff}} \approx 4\pi(\sigma_{\text{O}} + \sigma_{\text{O2}})D/\sqrt{2}, \tag{21}$$

with the diffusion coefficients given in Tables I–III.

The resulting values of k_{diff} at $[\text{M}] = 10^{22}\ \text{cm}^{-3}$ near 100 K are equal to $k_{\text{diff}} \approx 3\times 10^{-11}\ \text{cm}^3\ \text{s}^{-1}$. With increasing temperature, the corresponding values of k_{diff} in our temperature range increase approximately as k_{diff} $([\text{M}] = 10^{22}\ \text{cm}^{-3}) \propto T$. Inspecting Fig. 7 these properties of k_{diff} suggest that the high density leveling of k at $T \approx 100$ K can also be due to a transition to diffusion control and not to the approach of the high pressure limit k_{10} (which then should be larger than $k_{\text{diff}}([\text{M}] = 10^{22}\ \text{cm}^{-3}) = 3\times 10^{-11}\ \text{cm}^3\ \text{s}^{-1}$). The temperature dependence of k_{diff} would explain why no sign of a leveling of k is observed at $T > 200$ K and $[\text{M}] \leqslant 2\times 10^2\ \text{cm}^{-3}$. (We note that k_{10} only weakly depends[9,31] on T as long as adiabatic zero-point barriers can be neglected.)

Isotope enhancements in ozone recombination: The observed heavy isotope enrichments in ozone recombination[22–25] probably cannot be explained in terms of the ET and RC mechanisms. Isotope effects in the various factors contributing to the energy transfer mechanism, e.g., in the density of states, certainly are too small to account for the isotope enrichments. Likewise, Eq. (7) does not contain contributions with marked isotopic sensitivity. Larger isotope effects are expected if symmetry rules come into play and nuclear spin has to be accounted for. The investigation of the corresponding symmetry effects has to be done on a state-to-state level.[43] For collisions of ^{17}O with $^{17}\text{O}_2$ in comparison to $^{16}\text{O} + {}^{16}\text{O}_2$-collisions, this discussion has been done in Ref. 43: even or odd rotational levels of O_2 require different correction factors to the "symmetrized" statistical rate constants. Electronic excitation complicates the situation.[44] We do not intend to go into the details here, but we note that the heavy isotope enhancement effects disappear with increasing pressure[24] in a range where the EE–RC mechanism becomes dominant according to the present work. A detailed discussion of these effects, in particular of nuclear-spin selective electronic rotational couplings, such as discussed in Ref. 45, is far beyond the scope of the present article.

V. CONCLUSIONS

The good agreement of the maximum rate constants, observed in this work, with calculated rate constants for the diffusion-controlled reaction appears quite satisfactory. It suggests that the high density transition to a diffusion-controlled reaction at liquid densities is well characterized. The S-shaped structures of the density dependence of the rate constants at various temperatures and in various bath gases are more difficult to interpret. We have also had difficulties in accounting for the strong increase of the low pressure rate constants with decreasing temperature. Our present work suggests contributions from the energy-transfer mechanism in the bath gas He and from the radical-complex mechanism in the bath gases Ar and N_2, which at higher densities, are increasingly dominated by contributions from a mechanism involving metastable electronic states of ozone. It appears that the collision-induced transition from these states to the electronic ground state of ozone is strongly enhanced by complex formation of the metastable ozone with the bath gas. A confirmation of this hypothesis has to wait for precise quantum-chemical calculations of the potentials of metastable ozone, most probably of the $\text{O}_3(^3B_2)$ state. There is the possibility that the different pathways of ozone recombination and dissociation, involving different electronic states, are responsible for isotope enhancement effects. Again, a proof of this hypothesis has to wait for more detailed quantum-chemical calculations of ozone electronic states.

ACKNOWLEDGMENTS

We are grateful to M. Thiemens for communicating his ozone isotope enrichment results prior to publication. Financial support of this work by the Deutsche Forschungsgemeinschaft (SFB 93 "Photochemie mit Lasern") is gratefully acknowledged.

[1] J. Troe, Annu. Rev. Phys. Chem. **29**, 223 (1978).
[2] L. P. Walkauskas and F. Kaufman, *Fifteenth International Symposium on Combustion* (The Combustion Institute, Pittsburgh, 1974), p. 691.
[3] W. T. Rawlins, G. E. Caledonia, and R. A. Armstrong, J. Chem. Phys. **87**, 5209 (1987).
[4] R. Atkinson, D. L. Baulch, R. A.Cox, R. F. Hampson, J. A. Kerr, and J. Troe, J. Phys. Chem. Ref. Data **18**, 881 (1989) and earlier evaluations by this group.
[5] J. Troe, J. Chem. Phys. **87**, 2773 (1987).
[6] A. E. Croce and J. Troe, Int. J. Chem. Kinet. **16**, 1519 (1984).
[7] I. W. M. Smith, Int. J. Chem. Kinet. **16**, 423 (1984).
[8] C. J. Cobos, H. Hippler, and J. Troe, J. Phys. Chem. **89**, 1778 (1985); J. E. Dove, H. Hippler, and J. Troe, J. Chem. Phys. **82**, 1907 (1985).
[9] J. Troe, *Twenty-second International Symposium on Combustion* (The Combustion Institute, Pittsburgh, 1988), p. 843.
[10] J. Troe, J. Phys. Chem. **90**, 357 (1986); J. Schroeder and J. Troe, Annu. Rev. Phys. Chem. **38**, 163 (1987).
[11] B. Otto, J. Schroeder, and J. Troe, J. Chem. Phys. **81**, 202 (1984).
[12] H. Hippler, V. Schubert, and J. Troe, J. Chem. Phys. **81**, 3931 (1984).
[13] J. I. Steinfeld, S. M. Adler-Golden, and J. W. Gallagher, J. Phys. Chem. Ref. Data **16**, 911 (1987).
[14] A. J. Stace and J. N. Murrell, J. Chem. Phys. **68**, 3028 (1978); A. Gelb, J. Phys. Chem. **89**, 4189 (1985).
[15] J. R. Locker, J. A. Joens, and E. J. Bair, J. Photochem. **36**, 235 (1987).
[16] P. J. Hay and T. H. Dunning, J. Chem. Phys. **67**, 2290 (1977).
[17] K.-H. Thunemann, S. D. Peyerimhoff, and R. J. Buenker, J. Mol. Spectrosc. **70**, 432 (1978).
[18] C. W. Wilson and D. G. Hopper, J. Chem. Phys. **74**, 595 (1981).

[19] P. G. Burton, J. Chem. Phys. **71**, 961 (1979).

[20] R. O. Jones, J. Chem. Phys. **82**, 325 (1985).

[21] P. J. Hay, T. H. Dunning, and W. A. Goddard, Chem. Phys. Lett. **23**, 457 (1973); D. Grimbert and A. Devaquet, Mol. Phys. **27**, 831 (1974).

[22] J. E. Heidenreich and M. H. Thiemens, Geochim. Cosmochim. Acta **49**, 1303 (1985); J. Chem. Phys. **84**, 2129 (1986).

[23] J. Wen and M. H. Thiemens, Chem. Phys. Lett. (in press).

[24] M. Thiemens and T. Jackson, Geophys. Res. Lett. (in press).

[25] J. Morton, J. Barnes, B. Schueler, and K. Mauersberger, J. Geophys. Res. **95**, 901 (1990).

[26] R. Rahn, Ph. D. thesis, Göttingen, 1990.

[27] D. C. Astholz, A. E. Croce, and J. Troe, J. Phys. Chem. **86**, 696 (1982).

[28] H. Hippler and J. Troe, Ber. Bunsenges. Phys. Chem. **75**, 27 (1971).

[29] J. Troe, J. Chem. Phys. **66**, 4745, 4758 (1977); J. Phys. Chem. **83**, 114 (1979).

[30] H. Endo, K. Glänzer, and J. Troe, J. Phys. Chem. **83**, 2083 (1979).

[31] C. J. Cobos and J. Troe, J. Chem. Phys. **83**, 1010 (1985).

[32] M. Heymann, H. Hippler, D.Nahr, H. J. Plach, and J. Troe, J. Phys. Chem. **92**, 5507 (1988); H. Heymann, H. Hippler, H. J. Plach, and J. Troe, J. Chem. Phys. **87**, 3867 (1987).

[33] J. L. Durant and F. Kaufman, Chem. Phys. Lett. **142**, 246 (1987).

[34] E. Luzzatti, F. Pirani, and F. Vecchiocattivi, Mol. Phys. **34**, 1279 (1977); V. Aquilanti, G. Liuti, F. Pirani, F. Vecchiocattivi, and G. G. Volpi, J. Chem. Phys. **65**, 4751 (1976); V. Aquilanti, R. Candori, E. Luzzatti, F. Pirani, and G. G. Volpi, J. Chem. Phys. **85**, 5377 (1985).

[35] B. Brunetti, G. Liuti, E. Luzzatti, F. Pirani, and F. Vecchiocattivi, J. Chem. Phys. **74**, 6734 (1981).

[36] D. L. Bunker and N. Davidson, J. Am. Chem. Soc. **80**, 5090 (1958).

[37] H. S. Johnston, *Gas Phase Reaction Rate Theory* (Ronald, New York, 1966).

[38] P. S. Dardi and J. S. Dahler, J. Chem. Phys. **93**, 242 (1990).

[39] C. J. Hochanadel, J. A. Ghormley, and J. W. Boyle, J. Chem.Phys. **48**, 2416 (1968).

[40] J. F. Riley and R. W. Cahill, J. Chem. Phys. **52**, 3297 (1970).

[41] M. G. Sceats, Chem. Phys. **96**, 299 (1985).

[42] J. M. Dawes and M. G. Sceats, Chem. Phys. **96**, 315 (1985).

[43] M. Quack, Mol. Phys. **34**, 477 (1977); Ph. D. dissertation, EPF Lausanne, 1975.

[44] E. E. Nikitin and J. Troe, J. Chem. Phys. **92**, 6594 (1990).

[45] M. M. Graff and A. F. Wagner, J. Chem. Phys. **92**, 2423 (1990).

[46] O. Klais, P. C. Anderson, and M. J. Kurylo, Int. J. Chem. Kin. **12**, 469 (1980).

[47] C. L. Lin and M. T. Leu, Int. J. Chem. Kin. **14**, 417 (1982).

[48] I. Arnold and F. J. Comes, Chem. Phys. **42**, 231 (1979).

[49] R. E. Huie, J. T. Herron, and D. D. Davis, J. Phys. Chem. **76**, 2653 (1972).

[50] W. M. Jones and N. Davidson, J. Am. Chem. Soc. **84**, 2868 (1962).

[51] R. E. Center and R. T. V. Kung, J. Chem. Phys. **62**, 802 (1975).